Thermal Emission Microscope Studies of Cesium Surface Ionization on Porous Refractory Metals

D. M. Jamba and O. K. Husmann

Citation: Journal of Applied Physics **38**, 2630 (1967); doi: 10.1063/1.1709960
View online: http://dx.doi.org/10.1063/1.1709960
View Table of Contents: http://scitation.aip.org/content/aip/journal/jap/38/6?ver=pdfcov
Published by the AIP Publishing

Thermal Emission Microscope Studies of Cesium Surface Ionization on Porous Refractory Metals*

D. M. JAMBA AND O. K. HUSMANN†

Hughes Research Laboratories, Malibu, California

(Received 30 August 1966; in final form 1 February 1967)

Quantitative thermal emission microscope studies of cesium surface ionization on porous tungsten emitters show under clean surface conditions a surface migration length in the 2-μ range. The migration length from the pore exit is under this condition fairly independent of the flow rate per pore and the emitter temperature. It is therefore concluded that 10^7 pores/cm^2 (traverse counting technique) yield maximum ionization efficiency on porous tungsten.

Clean surface conditions were checked by Richardson work function measurements with the built-in Faraday cage. Also, the ion-current transition pattern in the threshold region was used for judgement of the surface condition. In case of a contaminated surface, a smooth transition from high to low ion current with decreasing temperature was observed in contrast to the steep ion-current change-over in the threshold region under clean surface conditions. Also the surface migration length increased on the contaminated surface.

Molybdenum, sputtered onto the porous tungsten substrate, showed a uniform work function over the entire emitter area with $\phi = 4.20$ eV.

INTRODUCTION

A thermal emission microscope has been employed to investigate cesium ion emission patterns obtained from rear fed, porous refractory metals. Magnifications are calibrated in the range of 50 to 2000 times, and the electrostatic lenses were designed for minimum image distortion. For quantitative measurements of electron and ion emission, a current collector is placed in front of the phosphor. Current densities have been measured in areas as small as 1 μ in diameter. X–Y motion is used to scan the emitter surface. These investigations were made under clean surface conditions, as ascertained by the Richardson work function measurements with the Faraday cage. Ionization studies on clean porous tungsten in the flow-rate-limited range at ion current densities up to several milliamperes per square centimeter revealed that the areas around the pore exit are the cesium emission centers. The diameter of these centers decreases slightly with increasing emitter temperature at constant alkali flow rate (is $\sim$2 to 5 μ). In the threshold region of surface ionization the inner area of the expanding emission centers strongly increases the atom evaporation; the region of ion emission encircles this area. A similar pattern was observed on a molybdenum layer sputtered on the tungsten substrate.

MICROSCOPE RESOLUTION

Magnifications, on the order of 1000 to 2000 times, are necessary for the study of the ion emission pattern at the pore exits; they can be achieved by the combination of an electrostatic immersion and unipotential lens. Magnifications exceeding 10^2 require improved techniques in order to make full use of the theoretically possible resolution.[1]

$$\delta = E/\epsilon \text{ cm}^{-1}, \tag{1}$$

with δ in lines per centimeter. ϵ is the thermal energy of the ions or electrons, and E is the electric field at the emitter surface.

Electrolytic tank studies were made of the electric field E at the emitter surface; they included studies of ion trajectories under a number of conditions, such as variation of the emitter electrode distance and the applied potentials at the immersion lens (see Fig. 1). These studies indicated that the E-fields were on the order of 8 kV/cm in the ranges of operation and therefore the theoretical resolution is in the 0.1-μ range.

Ions with energies exceeding about 20 eV sputter the target material (see Berisch[2]). In particular, most of the phosphors are very sensitive to sputtering and, as in case of ZnS, lose their fluorescent characteristic very rapidly. The ZnSi phosphor performs somewhat better. Aluminum backing does not sufficiently reduce the sputtering rate. Phosphor lifetimes under ion bombardment are generally too short for the observations reported here.[3] On the other hand, image converters perform satisfactorily.[4,5] The most common form of image converter employs a secondary electron cathode in form of a 500 (maximum 1500) mesh nickel grid at distance d from and parallel to the aluminum backed phosphor. The resolution of this converter is

$$\delta = 4d(U_e/U_B)^{1/2} \text{ mm}, \tag{2}$$

where d is the distance between the nickel grid and

* The work reported herein was supported by the National Aeronautics and Space Administration [AIAA Bull. 3, 41 (1966)].

† Now with Northrop Nortronics Applied Research Department, Newbury Park, California.

[1] G. Popp and W. Walcher, Ann. Phys. **20**, 293 (1957).

[2] R. Berisch, in *Ergebnisse der exakten Naturwissenschaften* (Springer-Verlag, Berlin, 1964), Vol. 35, pp. 297–422.

[3] D. G. Brandon, S. Raganathan, and D. S. Whitmell, Brit. J. Appl. Phys. **15**, 55 (1964).

[4] G. Moellenstedt and W. Hubig, Optik **15**, 538 (1958).

[5] M. V. Ardenne, *Tabellen z. Angewadt Physik* (VEB Deutscher Verlag der Wissenschaften, Berlin, 1962), Vol. I, p. 42.

the phosphor, about 5 mm, U_e is the mean energy of the secondary electrons released by ion impact on the nickel cathode, and U_B is the acceleration potential for the secondary electrons in the space between phosphor and grid. Here U_B is 10 kV, and secondary electron energy U_e at maximum yield is on the order of 2 eV. The converter resolution then is about 0.3 mm and the microscope total resolution in case of 10^3 magnification is 0.3 μ. If the electron converter secondary electron yield is $\eta \geq 1$, the phosphor light output is equal to or better than that experienced by electron bombardment. In general, the phosphor response to ions is smaller than that to electrons, except in the case of helium ions.[3] Ions which hit the nickel mesh under an angle smaller than 90° produce double images because of their ballistic trajectories in the retarding field between grid and phosphor. The ghost intensity exceeds that of the original image. If there is a sufficiently high ion retarding potential between the phosphor and the grid, the distance between the actual image and the ghost image can be minimized.

Magnetic fields affect the electron and ion trajectories particularly at low particle velocities such as those directly above the emitter. Here the electrons or ions are close to the magnetic field of the emitter heater spiral. The deflection angle θ is proportional to the filament magnetic field H at the emitter surface.

$$\sin\theta = 6.95\times 10^3\, L\times u_0 H/(MU)^{1/2}, \qquad (3)$$

where U is the thermal energy above emitter surface, M is the amu for electrons or ions, $u_0 = 4\times 10^{-7}$ V·sec·A^{-1}·m^{-1}, and $L = 10^{-5}$ m. H is in ampere turns per meter. The heater is located about 1 cm from the emitter surface, and the magnetic field at the emitter surface is reduced to approximately 1% of its original value. The average heater current is 10 A with a maximum at 15 A and a minimum at about 6 A. The electron or ion path length with thermal velocity is assumed to be about 10^{-5} m. With ×2000 magnification, we have

$$S = \sin\theta \times V = 7.85 \text{ mm}.$$

Therefore, ac heating cannot be used here, and dc heating (with low ripple) is necessary.

Furthermore, vibration of the emitter relative to the separately supported immersion lens electrodes and unipotential lens produces an effect similar to that of ac heating of the emitter; i.e., the microscope resolution becomes reduced. The electrostatic lens electrodes are all connected with the microscope walls; therefore, the problem is the natural frequency of the separately supported emitter electrode. Its natural frequency, as measured with a recorder pickup head, was at approximately 105 cps, neglecting higher harmonics. To isolate the microscope from the strong ground vibrations in the laboratory, a 1000-lb concrete block was mounted on coil springs as the microscope support. This shifted the natural frequency of the entire system into the low-frequency range, and the emitter is now better isolated from the laboratory floor vibration.

The resolution is further reduced by the development of space charge lenses on the emitter surfaces, in both the electron and ion emission states. Because we generally used fields of 8 kV/cm at the emitter surface, these space charge effects were nearly eliminated.[6] If there is some emitter surface roughness, the resolution and contrast are distorted because of distortion of the equipotential surfaces. A highly polished surface provides the best results.

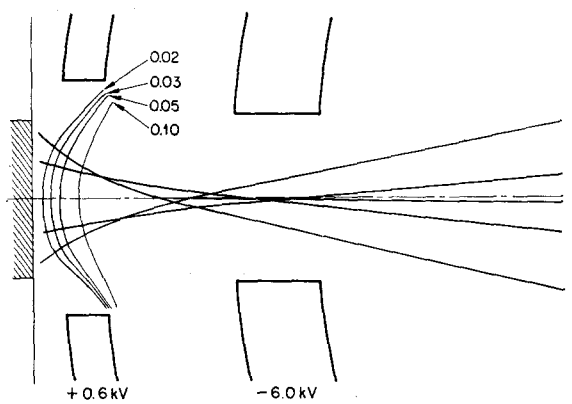

FIG. 1. Ion trajectories in the electrostatic immersion lens. The outer trajectories with shorter focal length are intercepted by the unipotential lens structure. With 6 kV at the front electrode and +600 V at the first electrode, the field at the emitter is 7.9 kV/cm.

THERMAL EMISSION MICROSCOPE

This ion microscope is built as an ultrahigh vacuum system, equipped with a 200-liter/sec ion pump. In accordance with our standard techniques, the system is evacuated during baking with a mercury diffusion pump, backed by a mechanical pump. A zeolite trap between the pumps prevents hydrocarbons from backstreaming into the vacuum chamber. The microscope is baked at about 200°C and the ion pump at maximum 150°C (ferrite ceramic magnets). After baking, the ion microscope is separated from the mercury diffusion pump by an all-metal valve. Only copper gaskets are employed. A liquid nitrogen cold trap in the upper part of the microscope helps to reduce the alkali vapor pressure during ion emission studies. Low alkali vapor pressure is essential for proper operation of the convertor unit.

The isolated emitter is mounted on an X–Y table which is movable by micrometer screws. The alkali supply and the emitter are heated separately. There is no valve in the alkali fuel line; therefore, some alkali comes out of the pores even if the electron emission is studied, and this alkali decreases the electron work

[6] G. V. Spivak, I. A. Pryankova, and N. N. Sedov, Bull. Acad. Sci. USSR, Phys. Ser. **24**, 648 (1960).

function at the pore exit. A heat sink, connected to the emitter support base and cooled from outside the microscope, allows the fuel side to be maintained at a reasonable low temperature if necessary.

The porous emitter temperatures have been calibrated with a Leeds and Northrup pyrometer in the temperature range between 1000° and 1800°K. The spectral emissivity depends on the surface roughness. In accordance with earlier measurements the spectral emissivity 0.6 was used in this calibration.[7] Window corrections are applied. The error in the temperature measurements does not exceed 10°K.

Minimum image distortion of the surface under investigation is of major importance both in work function studies of the emitter surface and in ion current density measurements. (This distortion can be checked easily with available emitter structure patterns. The two-dimensional pattern should be constant in size, independent of the place of observation on the phosphor.)

Maximum magnification with the electrostatic (immersion) lens is restricted to 130 times. Magnification was measured by comparison with the optically magnified image obtained using a Bausch and Lomb metallograph. Images of the same area were compared (a) in the light of electron emission and (b) optically. Therefore, our magnification data are based on the optical calibration of the microscope using a standard. Calibration was accomplished after the immersion lens distortion was minimized, using design data from Refs. 1, 8, and 9.

Figure 1 shows the different focal lengths for the inner and outer parts of the ion beam. Here the outer part of the ion beam does not contribute to the image because it is intercepted by the unipotential lens structure. In agreement with previous experience, the tank studies confirmed that both electrodes move away from the emitter with increasing acceleration potential, if the potential at the first electrode (opposite the emitter) remains constant. In this way, the focal length of the central beam is kept constant. The operation is conducted so that the first electrode usually is 600-V biased, repulsing electron or ion emission. The emission is then restricted to a very small area in the center of the electrode aperture. In addition, there is no electron current or ion current between the first electrode and the emitter, and sputtering of the first electrode material onto the emitter is therefore prohibited. This mode of operation offers the extra advantage of high magnification. Both electrodes are radiation-heated from the emitter, preventing clogging of the apertures, and they are gold plated to prevent electrostatic charge buildup.

In order to increase the magnification beyond that obtainable with an electrostatic immersion lens, a unipotential lens was added; its design parameters were in accord with those published by Pohlit *et al.*[10] (The design of low distortion unipotential lenses is well understood, as reviewed by Archard.[11]) This lens has a fixed position above the immersion lens and only the potential of its central electrode is variable. (It is connected with the emitter over a calibrated voltage divider.) The acceleration electrode of the immersion lens, as well as both outer electrodes of the unipotential lens, are on ground potential.

Figure 2 represents the total magnification of the ion microscope, based on the optical calibration of the immersion lens for various potentials, with the first electrode at 600 V (retarding potential for the emitted particles). The parameter in this plot is the percentage of the emitter voltage at the unipotential lens center electrode. With both lenses, a total magnification exceeding ×1800 is possible. By further decreasing the aperture and the critical dimensions of the unipotential lens, higher magnifications can be reached. Reasonable operation is achieved at acceleration potentials between 5 and 7 kV.

Here the ion microscope serves several purposes: With the Faraday cage it measures the electron work function of the emitter surface, including small patches and it quantitatively measures ion currents from small areas; it also observes the cesium distribution around the pore exits and measures the ion emission center radius.

The phosphor allows visual observation of the emission pattern and allows accurate placing of interesting

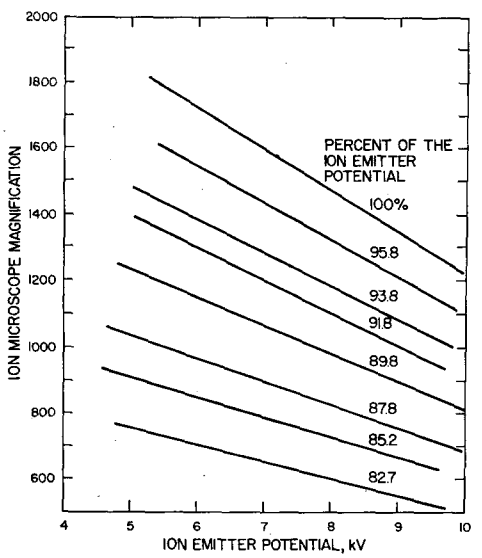

FIG. 2. Ion microscope calibration curves. The immersion lens first electrode is at +600 V. Parameter is the unipotential lens potential in percent of the emitter potential.

[7] O. K. Husmann, *Progress in Astronautics and Aeronautics*, (Academic Press Inc., New York, 1963), Vol. 9, p. 195.
[8] O. Brueche and A. Recknagel, *Elektronengeraete* (Springer-Verlag, Berlin, 1941), p. 256.
[9] W. Mecklenburg, Z. Physik **120**, 21 (1942–3).
[10] W. Lippert and W. Pohlit, Optik **9**, 456 (1952) and **10**, 447 (1953).
[11] J. O. Archard, Brit. J. Appl. Phys. **8**, 127 (1957).

emission zones under the Faraday cage. The Faraday cage is completely shielded to reduce noise background, and only a small circular 2-mm-diam inlet serves the current readings. A separate heater has been incorporated for re-evaporation of condensed alkali on its supporting insulator. The Faraday cup is located immediately beneath the converter grid, and therefore the calibrated magnifications can be used for computing the current densities. The current density j from a small surface area as measured by the Faraday cup is

$$j = iV^2/r^2\pi \text{ A/cm}^2, \quad (4)$$

where i is the measured current, V is the magnification (by optical calibration), and r is the radius of the Faraday cup aperture.

Presently, electron work functions up to 5.0 eV can be measured on 1-μ patches. Higher work functions require replacing the Faraday cage with an electron multiplier (with porous metals, the maximum obtainable temperature is about 1750°K). However, work functions exceeding 5.0 eV can be measured at low magnifications and, therefore, they represent an integrated surface area.

SURFACE IONIZATION STUDIES ON POROUS REFRACTORY METALS

The ion emission pattern on a porous refractory metal surface is of considerable interest in connection with the high ionization efficiencies required for electrostatic ion propulsion systems. The basic model of surface ionization at the pore exit was earlier discussed by one of the authors and is briefly repeated here[12]: With a solid surface, alkali is deposited from the vapor phase and there is statistically equal distribution of the alkali over the entire emitting surface; in contrast, on the porous surface the alkali is highly

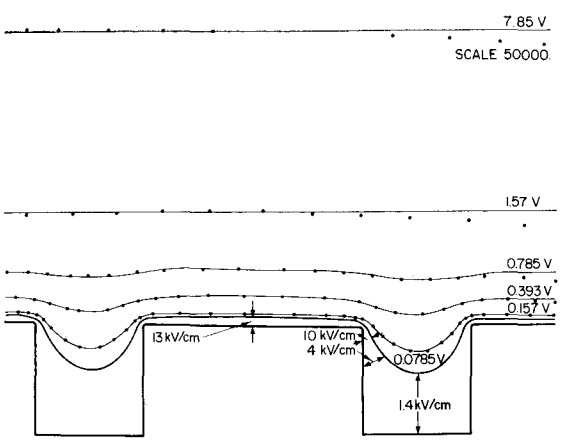

FIG. 3. Equipotential lines above an idealized porous emitter surface with 2-μ pore spacing and 1-μ pore diameter and pore depth. The applied potential is 10 kV. The actual potentials and fields are indicated.[15]

[12] O. K. Husmann, AIAA J. **1**, 2607 (1963).

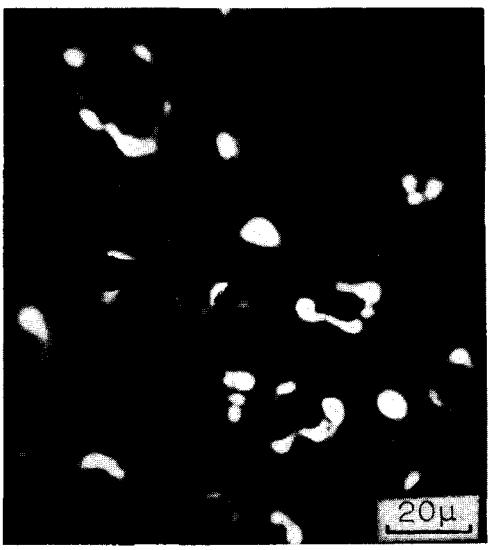

FIG. 4. Electron emission from sputter-deposited molybdenum after about 3 days operation at 1750°K. The crystal facets are partially cleaned up, as indicated by the dark inner area.

concentrated at the pore exit and consequently yields higher neutral efflux rates than the solid surface at the same average ion current density. Previous investigations of the neutral efflux rates on tungsten pellets with pore densities between 6×10^4 and 3×10^6 pores/cm^2 (traverse counting technique[13]) showed that the pore density governs the neutral efflux and that the pore diameter influences it only indirectly.[12] Porous tungsten pellets currently are limited to about 3×10^6 pores/cm^2, even when coated with 2.4-μ spherical tungsten powder of narrow size classification and a sintering density around 70% of theoretical.[14] The optimum pore density for various porous refractory metals and metal alloys (such as tungsten, rhenium, iridium, and tungsten–25% rhenium) still must be determined. Here the alkali ion emission center radius is the important parameter.[12] At 10^7 (equally spaced) pores/cm^2, the available migration length (without interception with alkali from a neighbor pore) is 1.58 μ. For 10^4 pores/cm^2, 50 μ are available. The surface migration length L is proportional to the temperature-dependent average alkali lifetime $\tau(T)$ and the diffusion coefficient $D(T)$.

$$L = [\tau(T) \times D(T)]^{1/2}. \quad (5)$$

As a first-order approximation, we assume that the alkali distributes equally around the pore exit with no preferential sites. The surface diffusion activation energy Q_d is low—about 11.5 kcal/mole. Geometrical thinning out of the surface coverage together with atom evaporation reduces the alkali surface coverage to a few percent as required for ion emission.[12]

The ion surface lifetime exponentially depends on the

[13] H. Muenzer and P. Schneiderhoehn, Heidelberger Beitr. Mineral. Petrog. **3**, 456–471. (1953).

[14] O. K. Husmann and R. Turk, AIAA J. **3**, 1653 (1965).

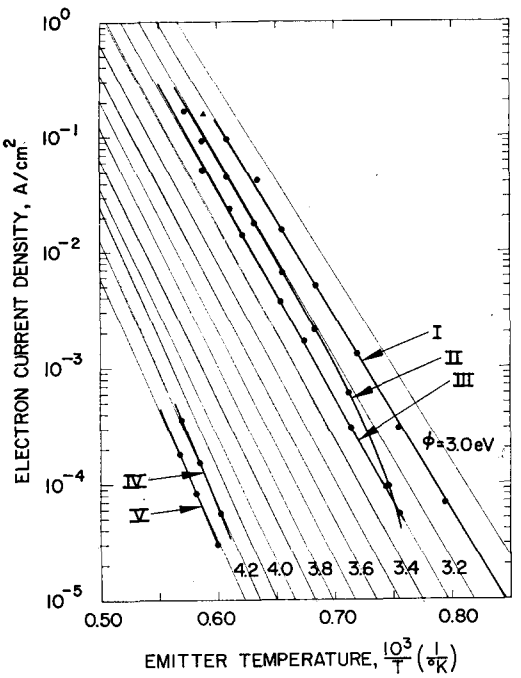

FIG. 5. Richardson work function measurement on molybdenum patches deposited on porous tungsten. Curves I, II, III, and IV were measured sequentially and illustrate the cleanup of the surface. Curve V was measured on a patch of the pellet support which is made of molybdenum.

ion desorption energy Q_i. This desorption energy is lowered by the electric field at the emitter surface with $-dQ_i=e(eE)^{1/2}$. Tank studies of the electric field at a model emitter surface magnified ×50 000, with pores of 1-μ diameter, 2-μ distance, and 1-μ pore depth (Fig. 3), indicate a field of 13 kV/cm with 7-kV extraction potential.[15] In the pore center, the field is 1.4 kV/cm; this increases to 10 kV/cm near the pore rim. At the pore rim, the field may reach 10^5 V/cm if the rim has a sharp corner. However, as the sharpness of the corner increases, its area and therefore its contribution to the ion current, decreases. Therefore, with regard to the surface area under consideration, we can conclude that the average field at the emitter surface does not exceed 13 kV/cm. Consequently, the decrease in cesium ion desorption energy is $-dQ=0.044$ eV.[15]

SURFACE CLEANUP PATTERN

According to the Saha equation, the ionization efficiency depends exponentially on the difference between the work function and the ionization potential. For a bulk contaminant the work function is frequently lower than that measured on the clean surface. In presence of oxygen or water vapor, however, the work function exceeds that of clean tungsten. (Here we refer to the clean polycrystalline surface.) As in previous work, thermionic emission data have been used also here for determining the cleanness of the emitter surface.[7,12] In case of gas adsorption on the emitter surface, cleanup is achieved by heating to sufficiently high temperature,[12] e.g., to 1800°K in case of oxygen adsorption. Small amounts of cesium hasten this cleanup at temperatures in the 1600°K range.

For bulk contaminants, the volume diffusion must be considered. As an example of such cleanup, one photograph from sputter deposited molybdenum is presented (see Fig. 4). The surfaces of all crystal facets have the same work function, and therefore the cleanup pattern of these about 20-mil-thick crystals is a good example. Note that the cleanup is seen in the change of thermionic work function. The first work function measurements on these crystal facets gave 3.1 eV, as computed from the Richardson plot, taken over a sufficiently wide temperature range. At a given temperature, all crystal facets show the same brightness. Here partial cleanup was achieved very slowly, over a period of a few days, while the emitter was kept at 1750°K. During this phase, the electron emission pattern on the facets changed. Instead of an equal brightness over the entire facet (with about 20×20-μ square surface), the central portion developed a higher work function and consequently became darker. The bright zone around this part can be seen in Fig. 4; this is characteristic for the entire sputtered molybdenum surface. During continued heating, the bright facet rim disappeared. Curves I, II, III and IV in Fig. 5 were measured sequentially. Curve V was measured on a patch of the pellet support, which is made of molybdenum. Finally, the work function stabilized at 4.2 eV (curve No. IV) after more than a week at 1750°K. For molybdenum, work functions between 4.15 and 4.44 eV have been reported.[16]

ION EMISSION STUDIES

The ion emission studies reported here were made on polycrystalline porous tungsten. For a better under-

TABLE I. Emitter temperatures and exposure times for ion-microscope photographs of surface ionization on sputter-deposited Mo.

Figure number	Exposure time (sec)	Emitter temperature (°K)
6c	150	1047
d	5	1063
e	5	1090
f	5	1143
g	5	1207
h	5	1320
i	5	1432
j	5	1513
k	5	1630
l	5	1742

[15] O. K. Husmann, Phys. Rev. **140**, A546 (1965); also, Bull. Am. Phys. Soc. **10**, 68 (1965).

[16] L. A. DuBridge and W. W. Roehr, Phys. Rev. **42**, 52 (1932)

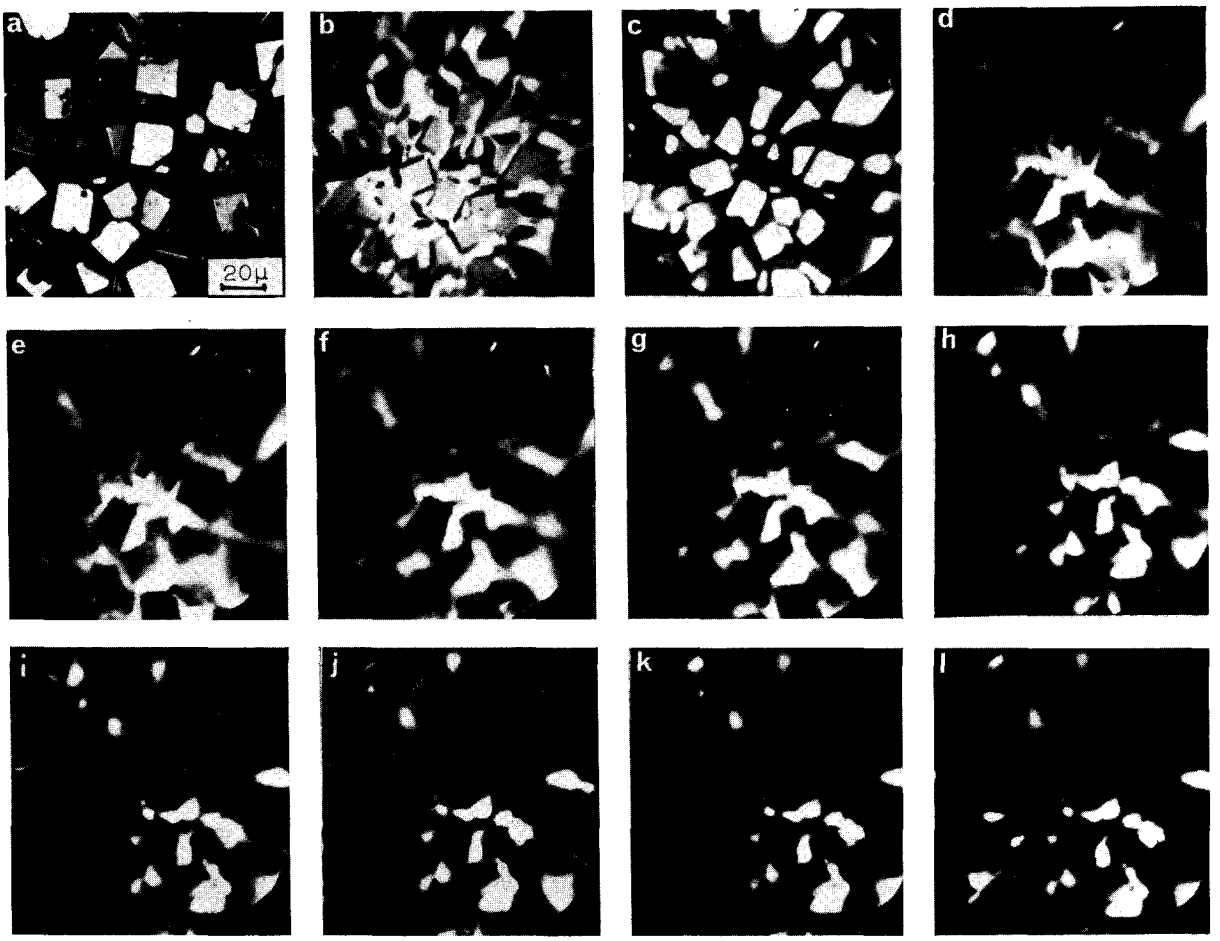

FIG. 6. Emission characteristics of sputter-deposited molybdenum. The magnification is ×300, and (a) is the optical image of the same surface area shown in the pictures (b) through (l). (b) is the electron emission pattern, and (c) through (l) represent the ion emission pattern with increasing temperature in the same sequence. (c) was taken in the threshold region of surface ionization (see Table I).

standing of the surface ionization mechanism inside the threshold region an additional study on molybdenum is reported. By means of Cs ion extraction from the porous tungsten pellet, molybdenum from the electrode opposite to the emitter was sputtered till an about 20-mil-thick porous Mo layer covered the porous tungsten substrate.

TABLE II. Emitter temperatures and exposure times for ion-microscope photographs (ϕ=3.75 eV).

Figure number	Emitter temperature (°K)	Exposure time (sec)
7a	1000	120
b	1015	60
c	1052	30
d	1080	30
e	1104	30
f	1183	25
g	1261	20
h	1336	20
i	1425	30
j	1511	30

On this porous molybdenum layer we observed cesium ion emission inside the threshold region for surface ionization from the crystal faces [Fig. 6(c)]. Obviously the dark areas between these crystal faces are overfed with cesium and therefore maintain too low a work function. A slight increase of the emitter temperature (here 16°K) transfers the ion emission into its saturation range, as the subsequent photograph shows. We see an inversion of the emission areas. The coverage between the crystal faces now is low enough to allow ion emission. There is no more cesium migration onto the crystal faces, [Fig. 6(d)–(l)] Table I. Similar to Marchant *et al.*[17] and also Forrester *et al.*,[18] simultaneous existence of different modes of operation has been observed here. However, in our experiments, such different modes were observed only under dynamic conditions i.e., when emitter tempera-

[17] A. B. Marchant, G. Kuskevics and A. T. Forrester, AIAA preprint 63018, AIAA Electric Propulsion Conference, Colorado Springs, March 1963. pp. 11–13.

[18] A. T. Forrester, G. Kuskevics and B. Marchant, Proceedings XIVth International Astronautical Congress, Paris, 1963.

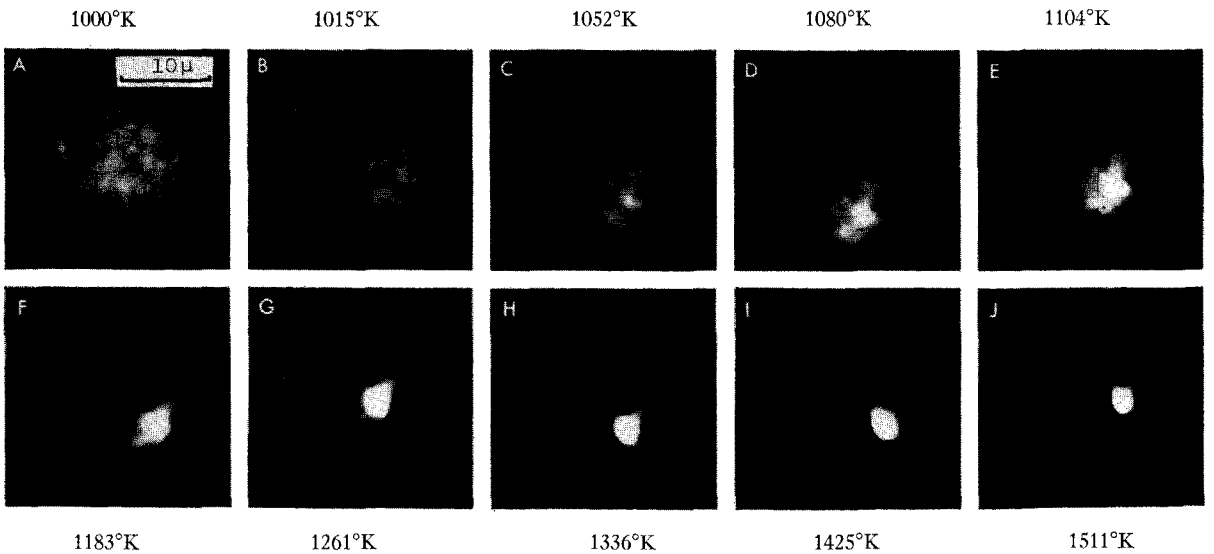

FIG. 7. Cesium ion emission from a single pore on porous tungsten observed over a temperature range of 1000° to 1511°K in the sequence (a) to (j) (see Table II). The work function is 3.75 eV.

ture was changing through the range close to the threshold for surface ionization. Under such condition the boundary between the ionization saturation region, the threshold region and the prethreshold region moves slowly over the screen.

Figure 6(a) is an optical view. Figure 6(b) shows this same area, in this case in the light of electron emission from the emitter surface. Note the same brightness of all crystal facets and the increased brightness in between; this increase results because of cesium diffusion and the lowered work function at the pore exit. All photographs were taken from the same emitter areas. In the saturation range, the ion emission center diameter shrinks at constant cesium flow rate with increasing emitter temperature. Table I gives the emitter temperatures and exposure times for Fig. 6. The exposure time for Fig. 6(c) was 30 times that of the other photographs. Double images at the figure periphery are visible.

Because ions are extracted from only a very small area, part of the evaporated cesium is intercepted by the molybdenum electrode opposite the emitter; this cesium is re-evaporated onto the emitter with statistical distribution, rather than accumulating around the pore exit. The cesium surface coverage on the remaining large emitter area, not shown in the photograph, is close to one monolayer of cesium atoms (note the positive ion retarding potential applied to the first electrode).

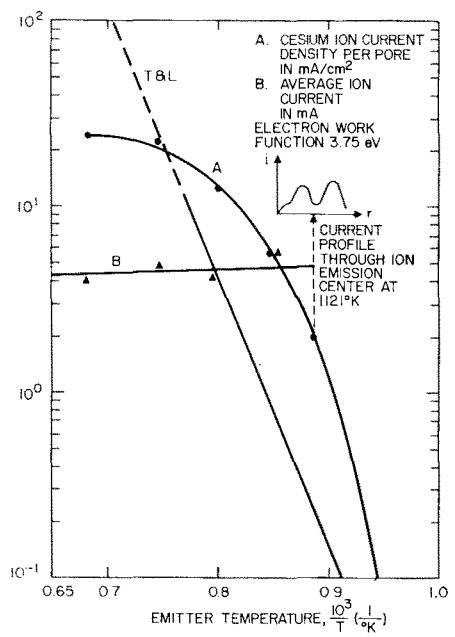

FIG. 8. Ion microscope studies of ion emission on tungsten from a single pore. $\phi = 3.75$ eV.

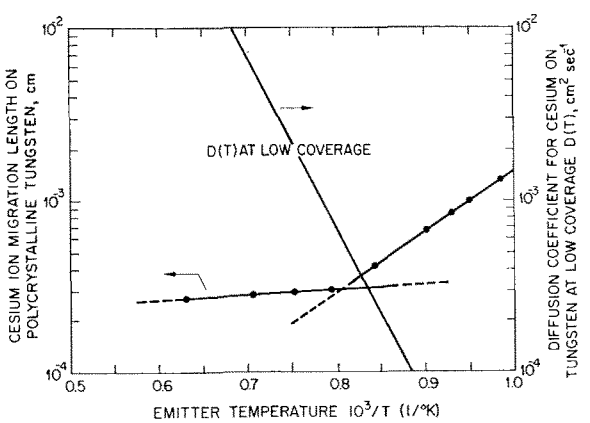

FIG. 9. Ion migration length and diffusion coefficient at low coverage for cesium on contaminated polycrystalline tungsten. $\phi = 3.75$ eV.

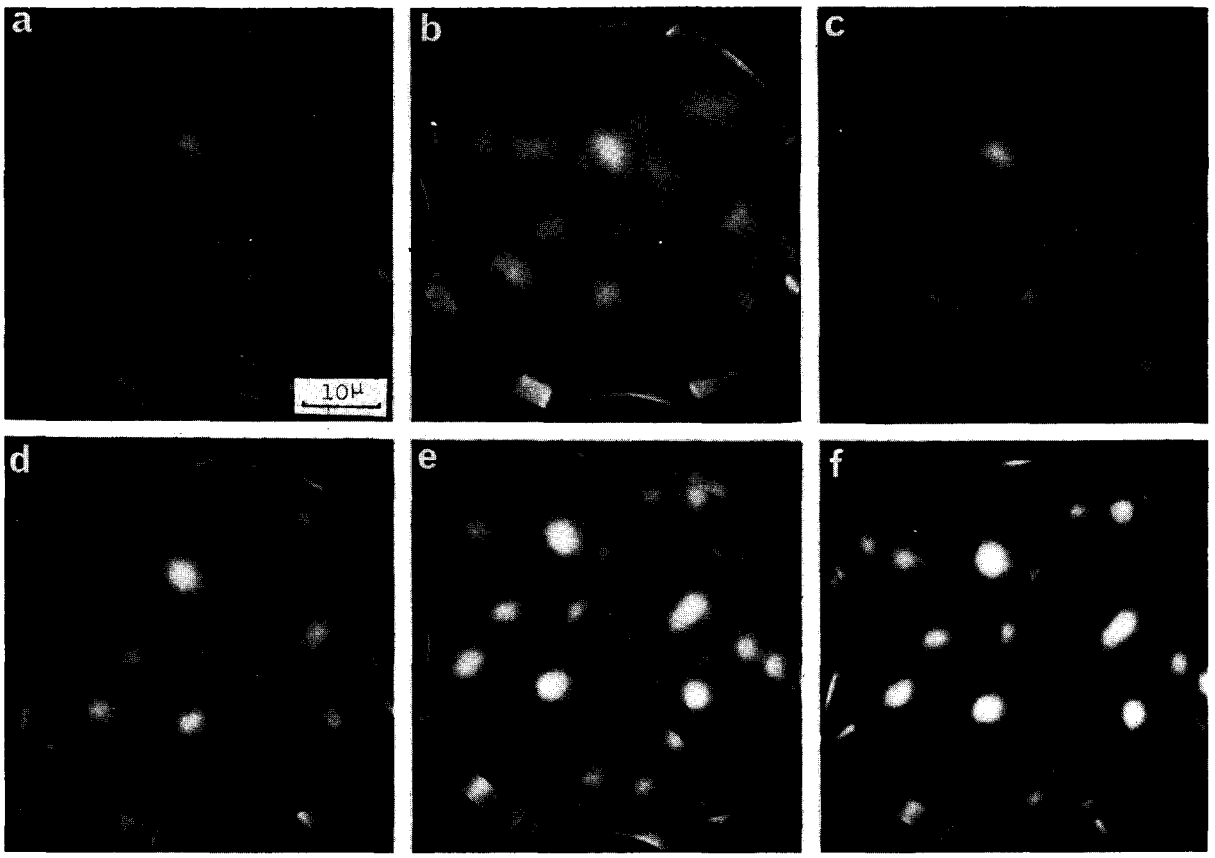

FIG. 10. Cesium ion emission from a clean porous polycrystalline W surface with increasing temperature from (a) to (f). The cesium flow rate is constant. The exposure time of (b) is twice that of the other pictures.

Ion microscope investigation of cesium ion emission from the porous tungsten under clean surface conditions yielded surprisingly small surface migration lengths; for contaminated surfaces this may be different, as discussed below.

A tungsten pellet with 3.75 eV-thermionic work function measured over a larger area of the emitter surface by Richardson plot yielded relatively small migration lengths in the saturation range. The single pore under investigation showed a somewhat higher cesium flow rate than the other pores. The exposure times and emitter temperatures for a series of photographs of this pore in the ion emission phase are given in Table II [see Fig. 7(a) through (j)]. The emission center radius expands strongly between 1104° and 1000°K. In Fig. 8 the average ion current for this emitter (curve B) and the ion current density per pore (curve A), as measured in connection with photographs similar to Fig. 7 are plotted ($\phi = 3.75$ eV). The cesium ion current density per pore, curve A of Fig. 8, was computed after measurement of the cesium ion current from this single pore taking the expansion of the ion emission area (Fig. 7) into account. Curve B represents the average ion current, as computed for the total emitter area. In contrast to the ion current density behavior on the clean tungsten surface (with the steep change-over from low to high ion current density), here we observe a smooth rolling over with no clearly defined threshold temperature. The data plotted in Fig. 8 were taken at a higher ion current density than the series of photographs in Fig. 7. An ion current scan through the ion emission center in the threshold temperature region is added in Fig. 8. Profiles crossing perpendicularly are very similar and shown an ion current minimum in the middle, as expected with a cesium overload. The ion current minimum in the center apparently was lower than indicated in the graph. The average ion current (curve B of Fig. 8) increases slightly with decreasing emitter temperature, as expected from the $T^{-1/2}$ dependence (straight line) of the cesium flow rate through the porous pellet. In Fig. 8 the threshold temperature for solid tungsten is added.[12] The measured threshold temperature is below this and indicates a low ϕ and contaminated surface.[15] Obviously, this surface is not carburized; for a carburized surface, we measured increased threshold temperatures compared with tungsten.[19] The ion current density per pore reaches 24 mA/cm², explaining the increased neutral efflux relative to that from vapor deposited cesium.

[19] O. K. Husmann, D. M. Jamba, and D. R. Denison, AIAA J., **4**, 273 (1966).

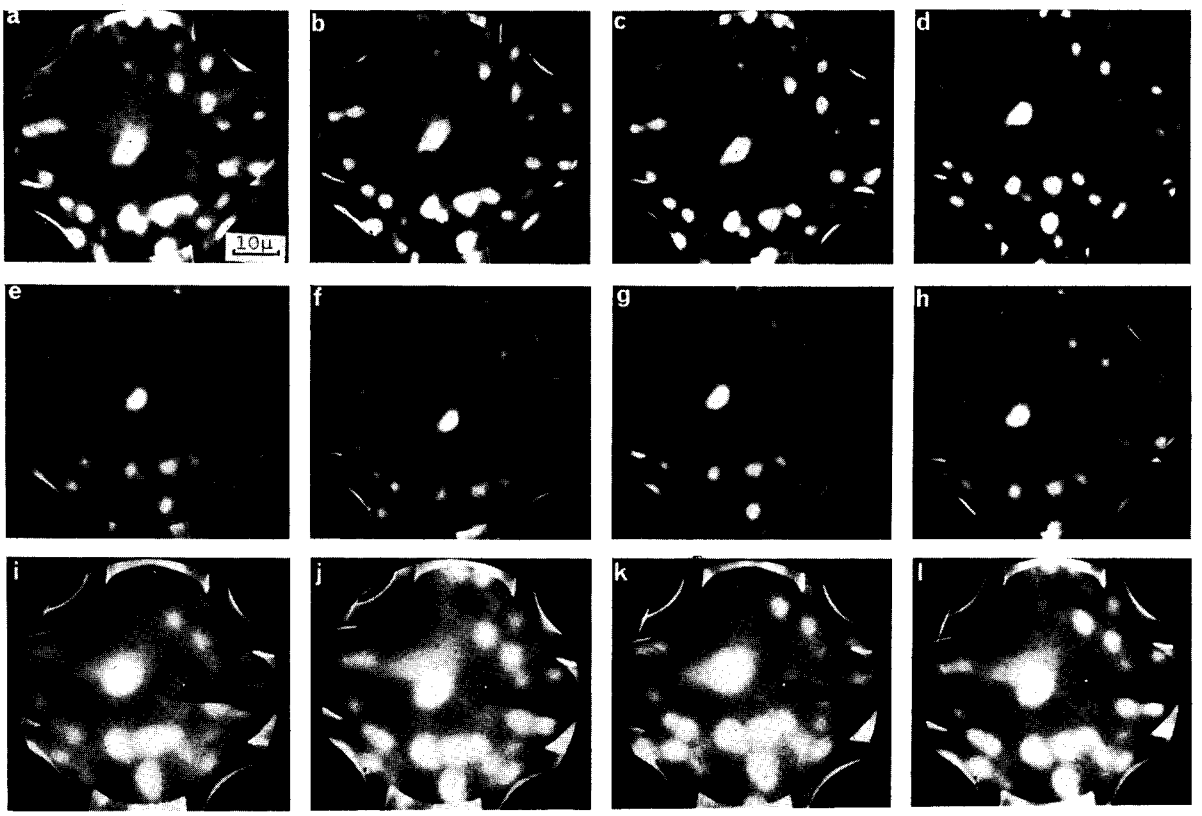

FIG. 11. Ion emission from clean porous tungsten for three cesium flow rates increasing from the first to the third line. The emitter temperatures increases from left to right.

If Fig. 7 is observed more closely in the low-temperature range [Figs. 7(a) through (d)] dark areas are seen between the bright spots. The distinctive pattern in 7(b) through (d) indicates the development of these dark areas. We may assume that the dark areas are overfed with cesium. According to Table II the images shown in Figs. 7(a) and (b) have, respectively, four times and twice the exposure time of the remaining photographs. Figures 7(a) through (e) were taken in the threshold region for surface ionization. A plot of the surface migration length (the radius of the ion emission area) is shown in Fig. 9. Two different modes of surface migration are observed: (1) In the high temperature (1250° to 2000°K) range, the surface migration is no more than a few microns, and this migration length L is expressed by

$$\log L = (3.54\times 10^2/T) - 3.782.$$

Below 1200°K, the surface migration length L is expressed by

$$\log L = (3.5\times 10^3/T) - 6.32.$$

L is in cm and T is in °K. At temperatures above

TABLE III. Exposure times and emitter temperatures for ion-microscope photographs.

Figure number	Exposure time (sec)	Emitter temperature (°K)
10a	0.5	1131
b	1.0	1156
c	0.5	1192
d	0.5	1252
e	0.5	1324
f	0.5	1450

TABLE IV. Exposure times, emitter temperatures, and cesium reservoir temperatures for ion-microscope photographs.

Figure number	Exposure time (sec)	Emitter temperature (°K)	Cesium reservoir temperature (°C)
11a	4	1240	85
b	4	1315	80
c	4	1381	75
d	4	1435	70
e	1	1240	140
f	1	1322	145
g	1	1379	145
h	1	1450	145
i	1	1238	180
j	1	1320	180
k	1	1392	180
l	1	1474	180

1250°K, the temperature-dependent surface diffusion coefficient [Eq. (5)] is expressed by $\log D(T) = -(9132/T)+4.192$, with

$$\tau = 1.77\times 10^{-12}\exp(11\,600 Q_i/T).$$

For clean polycrystalline tungsten $Q_i = 1.95$ eV, as reported earlier.[15] However, in connection with the threshold-temperature measurement here (see Fig. 8) the alkali ion desorption energy is lower than that for clean tungsten. It should be noted, that the emission center radius (equal to the migration length L) depends to some extent on the photographic exposure time, as indicated in Fig. 10(b). An error of L in the order of 20% is possible. Here D is only an approximation.

After slow cleanup for more than a week, the work function reached 4.29 eV and finally stabilized at 4.45 eV. A number of photographs were again taken for emitter temperatures from 1131° to 1430°K. Exposure times for these photographs are given in Table III. These photographs [Figs. 10(1) through (f)] make it evident that the surface migration length in this case is in the 2-μ range and is only slightly dependent on the emitter temperature. As would be expected in connection with $(1/r)$-surface-coverage dependence, the ion emission decreases strongly toward the rim of the emission center. For Fig. 10(b) the exposure time was doubled; the emission center expands slightly but the expansion is very limited, implying a stronger than $(1/r)$-decrease of the ion emission area radius.[12]

Figure 10(a) was taken close to the threshold of surface ionization. For equally spaced pores and 2-μ migration length, 6×10^6 pores/cm^2 would be the optimum pore density (traverse counting technique[13]). If the decrease of surface coverage of the emission center is considered, the pore density should actually be higher.

The emission center radius is not strongly dependent on the ion current density under clean surface conditions. Three series of emitter photographs are presented in Fig. 11. Here the magnification is kept constant, and all photographs are taken with $f = 1.9$. Figures 11(a) through (l) show the same emitter area for three different cesium flow rates. If the pictures of a single row are compared, a fairly constant spot size appears despite the steeply increasing cesium flow rate in the lower photographs. The different exposure time may contribute somewhat to the emission center size; however, if the images at emitter temperatures above 1400°K are compared, there is very little change in size. Furthermore, we know that the emission center does not expand very strongly above the visible size because of the steep decrease of the ion current density at the rim. All emission centers have nearly the same diameter. The cesium reservoir temperatures (see Table IV) are measured on the emitter support and are not necessarily the minimum temperatures of the cesium reservoir; however, they represent a good indication of the relative reservoir temperatures.

CONCLUSIONS

From the ion microscope investigation reported for clean-surface porous tungsten substrates, we conclude that the cesium migration length is in the 2-μ range radial to the pore exit. This migration length increases slightly with the cesium flow rate per pore. For maximum use of the available emitter surface area, it is suggested that tungsten pellets be developed with pore densities in the 10^7-pores/cm^2 range in order to insure a slight overlapping of emission centers.[20] It is recommended to expand these investigations to higher-work-function refractory metals and alloys, such as the tungsten–rhenium alloys, rhenium and perhaps iridium.

ACKNOWLEDGMENTS

The authors feel indebted to M. Wall and J. Becker for their contribution to the ion microscope construction.

[20] Traverse counting technique, as described in Ref. 13.